ACCELERATED PUBLICATION

Oxo-iron clusters in a bacterial iron-trafficking protein: new roles for a conserved motif

Haizhong ZHU*, Dmitriy ALEXEEV†[1], Dominic J. B. HUNTER*, Dominic J. CAMPOPIANO* and Peter J. SADLER*[2]

*School of Chemistry, University of Edinburgh, West Mains Road, Edinburgh EH9 3JJ, Scotland, U.K., and †Institute of Cell and Molecular Biology, Michael Swann Building, University of Edinburgh, Mayfield Road, Edinburgh EH9 3JR, Scotland, U.K.

We report a set of three 1.8–1.9 Å resolution X-ray crystal structures of *Neisseria gonorrhoeae* Fbp (ferric-ion binding protein): (i) open-cleft apo-Fbp containing bound phosphate, (ii) open-cleft mono-Fe Fbp capped by nitrilotriacetate, and (iii) open-cleft trinuclear oxo-iron Fbp, the first structure of an iron-cluster adduct of a transferrin. The nine independent molecules in the unit cells provide 'snapshots' of the versatile dynamic structural roles of the conserved dityrosyl iron-binding motif (Tyr^{195}-Tyr^{196}) which control the capture and, possibly, processing of iron. These findings have implications for understanding bacterial iron acquisition and dissimilation, and organic/mineral interfaces.

Key words: bacterial transferrin, dityrosyl motif, iron-binding protein, iron transport, oxo-iron cluster, X-ray crystallography.

INTRODUCTION

With few exceptions, bacteria require about 10^5–10^6 atoms of iron per generation to maintain a micromolar internal iron concentration, and iron increases the virulence of pathogenic strains ([1] and references cited therein). The earliest forms of life on earth experienced a reducing environment and utilized reduced (ferrous) iron, Fe^{2+} [2], but prokaryotes have adapted to ferric iron, Fe^{3+}, since intense UV radiation, anaerobic photosynthesis and oxygen generation have led to the oxidation of Fe^{2+}. The bioavailability of Fe^{3+} in aqueous environments is severely restricted by the insolubility of $Fe(OH)_3$, and micro-organisms have developed special mechanisms to capture Fe^{3+} [3]. The uptake of ferric iron by bacteria is regulated by Fur (ferric uptake regulation)-like proteins, which are responsive to both external and internal iron levels, and control the acquisition of iron from transferrins and haems, and from siderophores, which are produced to sequester iron and deliver it to specific membrane receptors [1,4–6,]. No specific system for the transport of polymeric (hydr)oxo iron species appears to have been identified, despite the prevalence of such forms of iron in the environment [7].

Fbp (ferric-ion binding protein), a single-chain 34 kDa protein, plays a key role in transporting Fe^{3+} from the outer membrane through the periplasm to the cytoplasmic membrane in Gram-negative bacteria, including many pathogens such as *Neisseria* and *Haemophilus* [8] (Figure 1). Fbp is produced by *Neisseria gonorrhoeae* in response to iron starvation [9], and is thought to reside as the apoprotein in the periplasm, where it can accept iron from outer-membrane receptors and transport it to cytoplasmic membrane receptors. The crucial role played by Fbp in iron uptake is illustrated by *N. gonorrhoeae fbp* mutants in which expression of Fbp is abolished: they are incapable of using non-haem iron ($FeCl_3$, iron citrate, transferrin and lactoferrin) for growth [10].

The X-ray crystal structure of recombinant holo-Fbp, as isolated, shows a single Fe^{3+} in a closed interdomain binding cleft with His^9, Glu^{57}, Tyr^{195}, Tyr^{196}, water and phosphate (the 'synergistic' anion) as iron ligands [11]. Phosphate can be replaced by other synergistic anions [12,13], which modulate the redox potential of bound iron [14]. Fbp shows strong structural homology with a single lobe of the bilobal proteins serum transferrin, ovotransferrin and lactoferrin, despite the lack of sequence identity [11,15]. Recently, we have characterized by X-ray crystallography [16] adducts of *N. gonorrhoeae* Fbp with bound oxo-Hf^{4+} clusters containing either three or five Hf^{4+} ions capped or uncapped by phosphate, clusters which resemble fragments of hafnium oxide minerals. Intriguingly, they lie in an open Fbp-binding cleft and are anchored only by Tyr^{195} and Tyr^{196} as protein ligands. Since the nature of the iron–Fbp complexes formed in the periplasm is unknown, and Fbp may even be able to sample iron directly in the external environment through exposure at the outer membrane [17], we have now investigated the possible formation of polynuclear iron–Fbp adducts. In the present study we report a set of three 1.8–1.9 Å (1 Å ≡ 0.1 nm) resolution X-ray structures of apo, mono-iron and oxo-tri-iron cluster forms of Fbp, which not only provide the first example of an iron-cluster adduct of a transferrin, but also 'snapshots' of the versatile dynamic role of a highly conserved dityrosyl motif.

EXPERIMENTAL

Materials

$Fe(NO_3)_3 \cdot 9H_2O$, PEG [poly(ethylene glycol)] 4000 and ammonium acetate were purchased from BDH. H_3NTA (nitrilotriacetic acid), atomic-absorption standards for Fe and S, and BNPP [bis-(4-nitrophenyl) phosphate] were obtained from Aldrich. Imidazole was purchased from Sigma, citric acid from Fisher, and PEG 1450 from Acros. $Na_3[Fe(NTA)_2] \cdot 5H_2O$ was prepared according to Clegg et al. [18], and diferric dicitrate $(Hpy)_2$-$[Fe_2(cit)_2(H_2O)_2] \cdot 2H_2O$ (where Hpy is protonated pyridine and cit is citrate) according to Shweky et al. [19].

Abbreviations used: BNPP, bis-(4-nitrophenyl) phosphate; cit, citrate; Fbp, ferric-ion binding protein; Hpy, protonated pyridine; NTA, nitrilotriacetate; PEG, poly(ethylene glycol); sTf, serum transferrin.

[1] Present address: Millennium Pharmaceuticals Ltd, Granta Park, Great Abington, Cambridge CB1 6ET, U.K.

[2] To whom correspondence should be addressed (e-mail P.J.Sadler@ed.ac.uk).

Co-ordinates have been deposited in the Protein Data Bank (accession code 1R1N).

Figure 1 Amino acid sequence of *N. gonorrhoeae* Fbp and conserved residues in homologues

(**A**) Sequence with grey highlights for residues conserved in organisms listed in (**B**), based on an Swiss Institute of Bioinformatics BLAST network service search [43] (exception, *Halobacterium* sp. $Gly^{229} \rightarrow Ser$). Fe ligands ($His^{9}$, Glu^{57}, Tyr^{195} and Tyr^{196}) in closed cleft form of *Neisseria* and *Haemophilus* Fe–P_i–Fbp are underlined in (**A**).

Protein preparations

We prepared recombinant *N. gonorrhoeae* Fe–P_i–Fbp and apo-Fbp as described previously [14]. To reload with iron, apo-Fbp (30–50 μM) in 10 mM Tris/HCl buffer, pH 8.0, was treated with a 10–50-fold molar excess of $Na_3[Fe(NTA)_2]$. After incubation at 310 K for 3 h, low-molecular-mass substances were removed on a PD-10 column, followed by ultrafiltration (Centricon YM-30 membrane, 30 kDa-molecular-mass cut-off; Millipore).

Crystallization of proteins

Large crystals of apo-Fbp were obtained in approx. 2 weeks at 277 K using the hanging-drop method. The well solution contained 30 % (w/v) PEG 1450, 0.4 M imidazole/HCl buffer, pH 7.2, and the drop contained 5 μl of well solution and 5 μl of 0.38 mM apo-Fbp in 0.1 M KCl. High quality apo-Fbp crystals for reactions with diferric citrate were obtained by freshly seeding saturated drops with crushed crystals of apo-Fbp. The drop contained 5 μl of well solution (30 % PEG 1450, pH 7.2) and 5 μl of apo-Fbp solution (0.4 mM in 0.1 M KCl). After 1 week at 277 K, the seeds were introduced into the drop with a glass fibre.

Large crystals of Fe–NTA–Fbp were obtained in approx. 2 weeks at 277 K using the hanging-drop method from a sample of apo-Fbp which had been reloaded with iron using excess $[Fe(NTA)_2]^{3-}$. The well solution contained PEG 4000 22 %, 0.4 M imidazole/HCl buffer, pH 6.9, and the drop contained 5 μl of the well solution and 5 μl of 0.4 mM Fe–Fbp in 0.1 M KCl.

For the preparation of Fe_3–Fbp crystals, 30 μl of an approx. 10 mM stock solution of $(Hpy)_2[Fe_2(cit)_2(H_2O)_2]$ in 30 % PEG 1450, 0.4 M imidazole/HCl buffer, pH 7.2, was added to 70 μl of the well solution described above containing apo-Fbp crystals. This addition caused the crystals to change from colourless to brown after approx. 20 min, and soaking was continued for a further 16 h.

Table 1 Crystallographic data and refinement statistics

Numbers in parentheses are for the highest resolution shell.

Parameter	Apo-Fpb	Fe–Fbp	Fe_3–Fbp
Wavelength (Å)	1.54	1.49	1.54
Resolution	1.88	1.80 (1.70 collected)	1.77
Refined twinning fraction (%)	30.1	44.0	44.1
Completeness (%)	99.9 (99.7)	91.4 (64.1)	96.5 (87.1)
I/Σ	19.1 (5.2)	11.1 (1.2)	7.1 (2.1)
R_{sym}* (%)	5.4	8.5	11.7
R_{cryst}† (%)/R_{free}‡ (%)	15.6/31.6	19.1/35.2	16.7/30.0
Root-mean-square deviations			
Bonds (Å)	0.007	0.007	0.006
Angles (°)	1.22	1.32	1.15
Average B-factors			
Protein (Å^2)	29.7	43.1	39.8
Water (Å^2)	35.3	37.6	35.8

* $R_{sym} = \Sigma|I_h - \langle I_h \rangle|/I_h$, where $\langle I_h \rangle$ is the average intensity over symmetry equivalent reflections.

† $R_{cryst} = \Sigma|F_{obs} - F_{calc}|/\Sigma F_{obs}$, where summation is over the data used for refinement.

‡ R_{free} was calculated using 3 % of data excluded from refinement.

X-ray data collection and structure determination (Table 1)

Crystals were flash-frozen in liquid N_2 and X-ray data for Fe–Fbp were collected on station 14.1 (Synchrotron Radiation Source, Daresbury Laboratory, Warrington, Cheshire, U.K.; $\lambda = 1.488$ Å) using an ADSC Quantum4 charge-coupled-device detector, and for apo-Fbp and Fe_3–Fbp at 100 K using a rotating anode generator RF591 ($\lambda = 1.542$ Å) where the anomalous contribution from Fe is approx. 3.1 $\bar{e}$ and P is approx. 0.4 $\bar{e}$ (comparable peaks visible for P and Met S of apo-Fbp), and processed and scaled using XDS (Fe_3–Fbp) [20] and HKL2000 (apo-Fbp and Fe–Fbp) [21]. Crystals belonged to the space group $P3_2$ (all cell dimensions close to $a = b = 145.7$ Å and $c = 114.2$ Å). The structures were solved using the methods described previously in [16,22], with 9 molecules (from A to I) in the asymmetric part of the unit cell. The positions of the Fe atoms in Fe_3–Fbp were revealed by difference anomalous Fourier synthesis calculated with the phases from the model refined without clusters. Peak heights were from 3–7.5 σ and clearly indicated the triatomic nature of the clusters, especially for molecules A, B, G and H. The clusters in the other molecules were disordered and the model for the density was based on that for A, B, G and H; all clusters were triatomic after further refinement. We were able to observe with confidence an anomalous signal from phosphate at the 3 σ level, together with the signal from Met^{308}, which confirms the presence of bound phosphate in apo-Fbp.

Phosphodiesterase activity

This was measured by using BNPP as a substrate and observing the increase in absorption at 400 nm due to formation of 4-nitrophenolate {[23]; ε_{400} (corrected to pH 8) = 18 205 $M^{-1} \cdot cm^{-1}$}, using 0.5 ml of solution in a 1-cm-pathlength quartz cuvette at 310 K on a Cary 300 UV-Vis spectrophotometer.

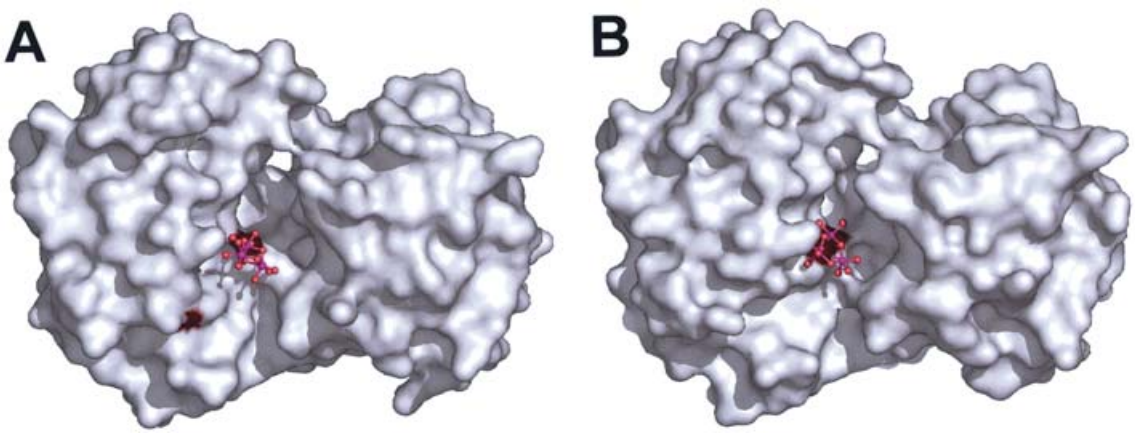

Figure 2 Trinuclear oxo-iron clusters in the open binding cleft of Fe_3–Fbp

Solvent-accessible surface models (grey; O atoms of Tyr^{195} and Tyr^{196} red) of (**A**) molecule F and (**B**) molecule A, with oxo-iron clusters as ball-and-stick representations (O, red; Fe, purple). Note the dark-red spot on the surface of molecule F in (**A**) indicating the hydroxy group of Tyr^{196}, which is flipped away from the cluster and exposed to the solvent (for details, see Figures 3C and 3D). In all the other eight molecules, Tyr^{196} is co-ordinated to iron as shown in (**B**). The cluster in molecule A sits deeper in the cleft.

RESULTS AND DISCUSSION

Typically, reactions of apo-Fbp with excess $[Fe(NTA)_2]^{3-}$ gave rise to proteins with Fe/protein molar ratios of 1.8–2.4:1 after removal of unbound complex and other low-molecular-mass substances. Cation-exchange chromatography of $Fe_{2.4}$–Fbp gave rise to two resolved peaks (results not shown), each with associated absorption at 280 and 480 nm, showing that both protein fractions contained Fe^{3+}–tyrosinate bonds. Crystallization of $Fe_{2.4}$–Fbp gave two kinds of crystals in the same crystallization drop: the first turned out to be Fe–NTA–Fbp, and the structure was solved (see below), whereas the second, thought to be iron-cluster Fbp, contained a very large unit cell (100 Å × 384 Å × 209 Å) and the structure was not readily solved. Therefore, we attempted to prepare iron-cluster Fbp by an alternative route, by soaking crystals of the apoprotein in diferric dicitrate, a procedure used recently for introducing iron into apo-FecA crystals [24]. Diferric dicitrate itself is thought to be an important donor of iron to cells, binding to the specific receptor FecA, which induces transcription of the *fecABCDE* operon.

Trinuclear oxo-iron clusters in Fbp

Colourless crystals of apo-Fbp soaked in a solution of diferric citrate $[Fe_2(cit)_2(H_2O)_2]^{2-}$ turned brown, and we determined the structure of the brown crystals at 1.8 Å resolution. Though the electron density does not reach atomic resolution, the maps clearly indicated the presence of tri-iron clusters. The iron atoms were confidently revealed both by the $|F_{obs} - F_{calc}|$, PHI_{omit} difference map and by the anomalous Fourier map, calculated with the phases PHI_{omit} from the model, refined with the binding cleft empty. The orientation of the cluster in the metal-binding clefts of the nine molecules A-I in the asymmetric part of the unit cell vary, but the overall shapes of all clusters in the $|F_{obs} - F_{calc}|$, PHI_{omit} difference map are very similar, and correspond well to Fe_3O_{13} tri-iron structural units. Such units are present in 19 entries in the Cambridge Crystallographic Database, and often form part of extended arrays in higher order iron aggregates. The oxygen atoms in Fe_3O_{13} units lie in approximately parallel layers with approximate closest-packing geometry. Examples include $[Fe_9O(cit)_8(H_2O)_3]^{7-}$ [25] and Fe_{19}-oxyhydroxide clusters encapsulated by N-(1-hydroxymethylethyl)iminodiacetate ligands [26]. All nine Fbp molecules in the asymmetric unit contain tri-iron clusters. Each cluster is situated in an open binding cleft (Figure 2), and contains a triangle of Fe^{3+} ions with each pair bridged by a μ_2-oxygen (Figures 3C and 3D). A central μ_3-oxygen co-ordinates to all three irons. Three additional terminal oxygen co-ordinate to each Fe^{3+} of the tightly bridged Fe_3O_4 unit and complete the oxygen co-ordination shell of the octahedral iron atoms within the Fe_3O_{13} cluster. We manually manoeuvred the Fe_3O_{13} clusters (taken from the Cambridge Crystallographic Database) into the difference maps for all molecules A–I and adjusted them to match the electron density.

In all of the 9 molecules in the asymmetric part of the unit cell, except F, the hydroxy group of Tyr^{196} is deprotonated and occupies the position of the central μ_3-oxygen in the co-ordination sphere of the tri-iron cluster (Figure 3D). Surprisingly, in molecule F this tyrosine (Tyr^{196}) is turned away from the cluster and a μ_3-oxide is recruited from water (Figure 3C). The co-ordination of the adjacent tyrosine (Tyr^{195}) varies much more widely. In molecules A, B, F, G, H and I, Tyr^{195} is directly co-ordinated to iron and appears to be deprotonated. In other molecules, it is not. Tyr^{195} forms a hydrogen bond with one of the terminal oxygen atoms of the cluster in molecules D and E, and with one of the bridging μ_2-oxygen atoms in molecule C. Also residues Ser^{139} and Asn^{175} make H-bond contacts with the bound cluster (Figure 3). None of the oxo tri-iron clusters bound to Fbp appears to contain bound citrate. This can be rationalized on the basis of the known aqueous solution chemistry of diferric dicitrate. Crystalline diferric dicitrate consists of two Fe^{3+} ions bridged by two alkoxide oxygen atoms of fully deprotonated citrate ligands [19]. The complex is stable in acidic solution at pH 2–3, in equilibrium with higher-order clusters, such as $[Fe_9O(cit)_8(H_2O)_3]^{7-}$ [25]. In 1:1 Fe^{3+}/citrate solutions, citrate is known to dissociate from Fe^{3+} at pH 4 and above to give (hydr)oxy-iron polymers (particles) with citrate ions bound to the surface, so preventing precipitation [27]. This chemical transformation is readily observable by UV-visible spectroscopy: the colour of the solution changes from yellow–green at pH 2–3 to red–brown at pH 8. We find that the rate depends on the exact conditions (higher with hydroxide addition than in buffers, and on exposure to light; results not shown). Since ferric citrate is widely used in studies of iron uptake by cells under

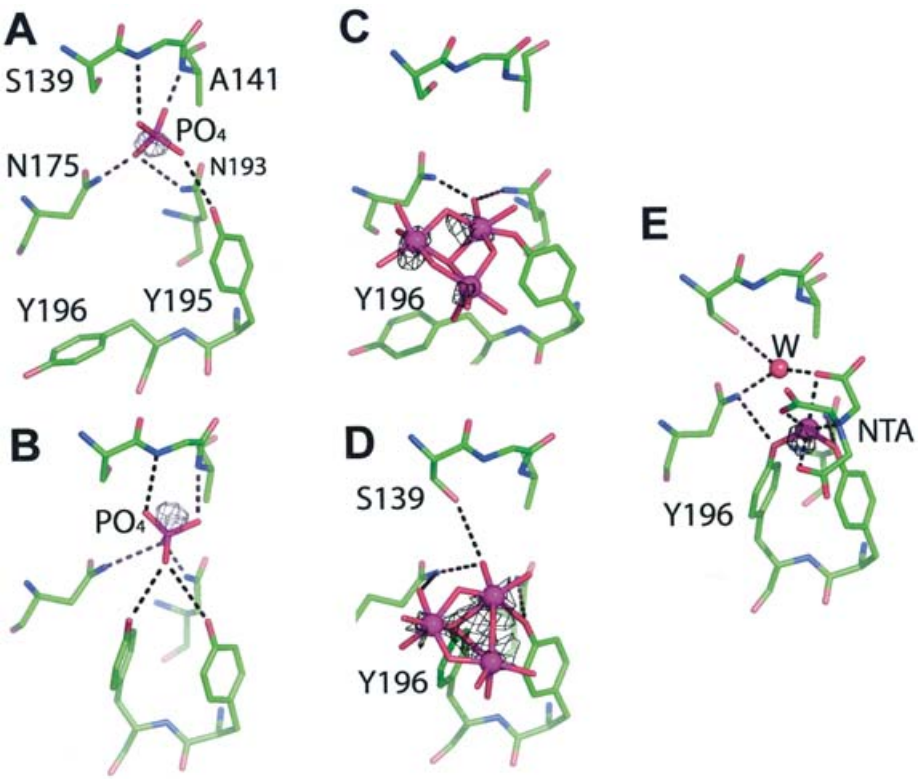

Figure 3 Dityrosyl motif (Tyr^{195}-Tyr^{196}) in apo-Fbp, Fe_3–Fbp and Fe–NTA–Fbp

Anomalous electron density maps are contoured at the 3 σ level and indicate ligand positions. (**A**) Molecule F of apo-Fbp. Tyr^{196} is flipped out and the phosphate is bound to the N-terminus of an α-helix. (**B**) Molecule A of apo-Fbp. Both Tyr^{196} and Tyr^{195} are H-bonded to the phosphate. (**C**) Trinuclear oxo-iron cluster in molecule F of Fe_3–Fbp. There is a central μ_3-bridging oxide, Tyr^{195} is co-ordinated to one Fe^{3+} and Tyr^{196} is flipped out. (**D**) Trinuclear oxo-iron cluster in molecule A of Fe_3–Fbp. Both tyrosines co-ordinate to the cluster. Tyr^{196} provides the central μ_3-bridging oxygen and Tyr^{195} is monodentate. (**E**) The mononuclear Fe site in Fe–NTA–Fbp. Fe is bound to both tyrosine residues in all the nine molecules (A–I). The anomalous map is contoured at the 6 σ level; the iron is very well-ordered.

a variety of conditions, further studies on its speciation in culture medium and in cells are warranted. In a recent 2.5 Å resolution X-ray study [24], crystals of the outer membrane iron receptor apo-FecA soaked in ferric citrate at pH 8 appeared to capture diferric dicitrate itself, triggering a conformational change of the extracellular loops of FecA and closing the external pocket. It would be interesting to investigate whether FecA can bind oxo-iron clusters and whether these can trigger receptor gating. It is notable that FecA contains several Tyr–Tyr sequences.

Open-cleft mono-iron Fbp

X-ray crystallography showed that crystallization of the product from the reaction of apo-Fbp with $[Fe(NTA)_2]^{3-}$ gives rise not only to crystals of the cluster adduct Fe_3–Fbp, but also to crystals of the mono-iron adduct Fe–NTA–Fbp. This contains a single Fe^{3+} only bound to Tyr^{195} and Tyr^{196} as protein ligands, and also to tetradentate NTA in an open protein cleft (Figure 3E). Fe^{3+} is shielded from solvent by the chelated NTA ligand in much the same way as by bound EDTA in the recently reported structure of *Haemophilus influenzae* Fe–EDTA–Fbp [28], in which His^9 (an Fe^{3+} ligand in closed-cleft holo-Fe–P_i–Fbp) had been mutated to Gln. Our present work therefore shows that open-cleft mono-Fe–Fbp is stable even for the native protein. An open-cleft form of hen Fe–(N-lobe)–ovotransferrin prepared by soaking crystals of the apo-protein with Fe–NTA has been reported [29], also with iron bound only to two Tyr ligands (Tyr^{92} and Tyr^{191}) and tetradentate NTA. The authors concluded that the open-cleft conformation was trapped by crystal packing forces. Since our Fe–NTA–Fbp was crystallized from preformed complex, the cleft opening observed here does not appear to depend on such packing forces. In the X-ray structure of an adduct of an 18 kDa N-lobe domain-II fragment of duck ovotransferrin with bound iron and NTA [30], only one of the two tyrosine residues (Tyr^{194}) which bind iron in the cleft of the native duck protein is bound to Fe^{3+}, whereas the other (Tyr^{95}) is 3.8 Å away from iron. Such movements of the iron-binding tyrosine residues also observed in the work reported in the present study for intact bacterial transferrin (in Fe_3–Fbp and apo-Fbp, see below, Figure 4) are probably crucial for iron processing by transferrins. Clearly residues His^9 and Glu^{57} which bind to iron in holo-Fe–P_i–Fbp are not required for Fe^{3+} binding in an open cleft. The opening of the binding cleft of Fe–Fbp is likely to have a major effect on the reactivity of the bound iron.

Tyrosine movement in apo-Fbp

The versatile dynamic roles of the side chains of Tyr^{195} and Tyr^{196} are further evident from our 1.9 Å resolution X-ray structure of apo-Fbp. All 9 molecules in the asymmetric part of the unit cell of our crystal form contain bound phosphate, despite the lack of phosphate addition during the purification procedure. The high quality of the X-ray data allowed confirmation of the presence of phosphate by a strong peak in the anomalous density map (Figures 3A and 3B), comparable in height with the peak for the

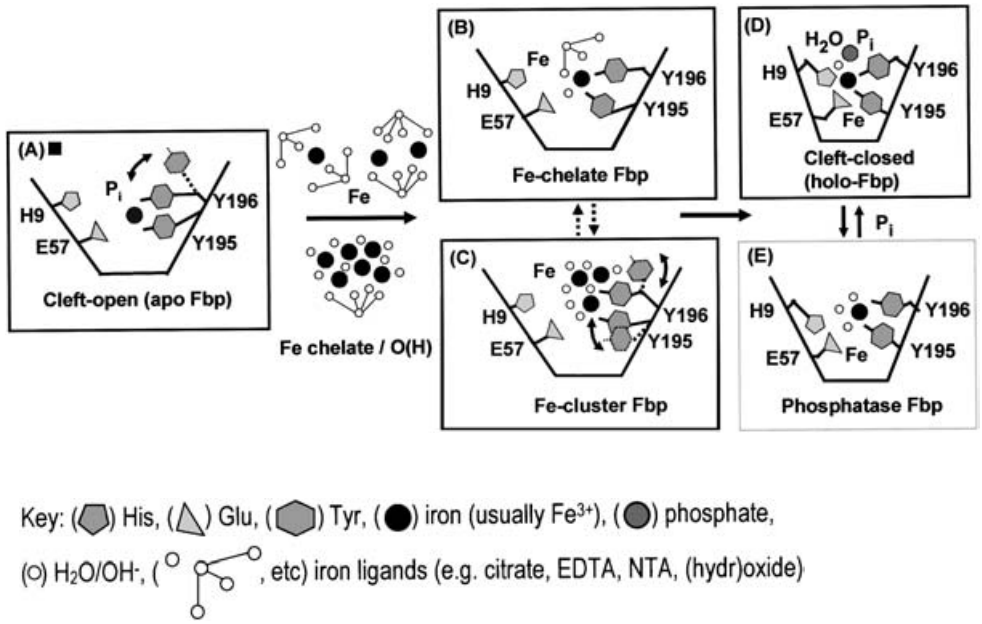

Figure 4 Uptake of iron into the binding cleft of bacterial transferrin

The diagrams illustrate the versatility of the dityrosyl motif (Tyr^{195}–Tyr^{196}) and are all based on X-ray evidence, except for (**E**). (**A**) Apo-Fbp with bound phosphate (Figures 3A and 3B, and [31]). The conformational flexibility of Tyr^{196} may play a role in guiding iron into the cleft.) (**B**) Open-cleft Fe–Fbp with iron bound to Tyr^{195} and Tyr^{196} and a chelating ligand {e.g. NTA (Figure 3E) or EDTA [28]}. (**C**) Fe_3–Fbp (Figures 3C and D) showing an open cleft with flexible roles for Tyr^{195} and Tyr^{196}. Enlargement of the cluster may be possible, as observed for hafnium [16]. (**D**) Closed cleft holo-Fbp with His^9 and Glu^{57} in addition to Tyr^{195} and Tyr^{196} as protein ligands for Fe^{3+}, together with the synergistic anion phosphate and water [11]. (**E**) An open-cleft Fe-Fbp with potential coordination sites for phosphate esters and subsequent hydrolysis. Multinuclear forms of Fbp may also be active.

S atom of the methionine residue. As for *H. influenzae* apo-Fbp [31], phosphate is specifically bound to the N-terminus of the helix which terminates in Ala^{141} and the phosphate oxygen atoms are within 3–4 Å of the oxygens of Tyr^{195} and Tyr^{196} (Figure 3B). Similar to the structure of Fe_3–Fbp, Tyr^{196} in molecule F of apo-Fbp is also flipped towards the entrance of the binding cleft, suggesting a potential role for Tyr^{196} in guiding iron complexes into the cleft. Evidently the two iron-binding tyrosine residues can have distinctly different roles within the binding cleft of Fbp, as has been illustrated for human transferrin by mutation of Tyr^{95} and Tyr^{188}, the metal-binding tyrosine residues in the N-lobe cleft [32] and for the duck NII domain fragment [30].

Phosphatase activity

We investigated whether Fe^{3+} in open-cleft Fbp is accessible and potentially reactive. We studied reactions of Fe–Fbp with BNPP, a model substrate for phosphatase activity [33]. No reactions were observed between BNPP and $[Fe(NTA)_2]^{3-}$ or apo-Fbp in Tris buffer, or with holo-Fe–P_i–Fbp in Hepes buffer. However, holo-Fbp from which bound phosphate had been removed by ultrafiltration in 50 mM Tris buffer [16] did cleave the phosphoester bonds of BNPP slowly (increase in absorption at 400 nm), consistent with the opening of the binding cleft on phosphate removal. Reloaded $Fe_{2.4}$–Fbp was also an active phosphatase. We determined a first-order rate constant of 5×10^{-6} s^{-1} for this sample (40 μM Fbp, 0.42 mM BNPP and 50 mM Tris buffer, pH 8.0, 310 K). This represents an increase in rate of BNPP hydrolysis by approx. $> 10^4$ compared with the spontaneous rate (too low to measure under our conditions; previously reported as 3×10^{-10} s^{-1} at 323 K, pH 7 [34]). It will be interesting to investigate the activity of various forms of iron Fbp and also the recognition of a range of potential natural substrates. Phosphatase activity could provide a mechanism for signalling iron status by coupling cluster breakdown and cleft closure around a single iron.

Implications for bacterial iron transport

Since Fe–Fbp has been characterized only as a mono-iron complex previously, it is has been assumed that iron is transported across the periplasm only as mononuclear centres. Our work shows that Fbp can readily bind oxo-iron cluster adducts, which therefore introduces the possibility that clusters, which are small fragments of (hydr)oxo iron minerals, could be involved in iron trafficking (Figure 4). Whether such clusters can be acquired directly from the external environment by periplasmic Fbp [35] (since it is known to have access to the outer surface of bacteria [17]), or can be assembled from uptake of mononuclear iron, remains to be investigated further. It is notable that in some bacteria FecA is a receptor for diferric dicitrate (the iron donor we used to form Fe_3–Fbp) and a database search revealed that nearly half of the bacteria which possess a Fbp homologue also possess a FecA homologue (Figure 1). FecA might therefore be considered as a possible donor of polynuclear iron to Fbp.

Fe_3–Fbp appears to be the first example of an oxo tri-iron centre in a metalloprotein. (Hydr)oxo-di-iron centres are well known, being present in, for example, ribonucleotide reductase, methane mono-oxidase and haemerythyrin [36], whereas ferritin has a particulate core of (largely) Fe(O)OH, taken up as Fe^{2+} and oxidized in gated pores in the protein coat [37,38]. Sulphide-bridged di-, tri- and tetra-iron clusters are found in ferredoxins. Ferredoxins have a multitude of diverse roles, including electron transport, and probably sustained early life in a highly reducing environment [39]. Oxo-iron clusters bound to Fbp may also have interesting redox activity. As well as playing a role in iron uptake in pathogens, Fbp could also be involved in iron acquisition by

iron dissimilatory bacteria, such as *Shewanella oneidensis* (Figure 1), which shuttles electrons from the cytoplasm to the outer membrane for the reductive breakdown of Fe^{3+} minerals [40]. *Shewanella* can adsorb and grow on fine-grained aggregates of ferrihydrite [41], but little is known about the proteins involved in the iron-uptake mechanism in this micro-organism.

The mobility and acid–base properties of the side chains provide the dityrosyl motif of bacterial transferrin with a potentially versatile role in the capture and release of iron (Figure 4). Although in most of the nine protein molecules A–I in the unit cell of Fe_3–Fbp the tri-iron cluster is anchored by Tyr^{196} as a triple-bridging ligand and by Tyr^{195} as a monodentate terminal ligand, either tyrosine residue can also act as a single arm anchor for the cluster. Hence the verstatile structural roles of these Tyr residues may provide facile mechanisms for iron uptake and release either as mono- or poly-nuclear centres.

It remains to be seen whether eukaryotic transferrins can also bind to iron clusters. In sTf (serum transferrin), the tyrosine residues which bind to iron in closed-cleft Fe–CO_3–sTf are well separated in the sequence [15] (95 and 188 in the N-lobe, 426 and 517 C-lobe) and not sequential as in Fbp. Either of these tyrosine residues could perhaps act as an anchor for an oxo-iron cluster under certain conditions. Notable, however, is the presence of a highly conserved dityrosyl motif in the N-lobe (Tyr^{95}–Tyr^{96}) of sTf. Perhaps this motif could also be functional in cluster recognition by sTF.

Studies of a wide range of bacteria should now enable exploration of the potential role of iron-cluster Fbp in perplasmic iron trafficking, so providing new insights into bacterial–mineral interfaces, virulence and the design of novel antibiotics. Intriguingly, we find that the oxophilic ion Zr^{4+}, a potential metallo-antibiotic, can block Fe^{3+} binding by Fbp and that even 1:1 mixtures of apo-Fbp and Zr^{4+} lead to the assembly of tri-zirconium clusters in the binding cleft [42].

We thank The Wellcome Trust (Edinburgh Protein Interaction Centre and Showcase Award), Darwin Trust (Fellowship for D. A.), Committee of Vice-Chancellors and Principals (Overseas Research Students Award for H. Z.), Wolfson Foundation and Royal Society for their support for this work, Dr Marjorie Harding (Edinburgh) for stimulating discussions, and Professor Bob Williams and Professor Malcolm Walkinshaw for their helpful comments on the manuscript.

REFERENCES

1 Raymond, K. N., Dertz, E. A. and Kim, S. S. (2003) Enterobactin: An archetype for microbial iron transport. Proc. Natl. Acad. Sci. U.S.A. **100**, 3584–3588
2 Frausto da Silva, J. J. R. and Williams, R. J. P. (1991) The Biological Chemistry of the Elements, pp. 14–18, Clarendon Press, Oxford
3 Crichton, R. R. (2001) Inorganic Biochemistry of Iron Metabolism, J. Wiley & Sons, Chichester
4 Ratledge, C. and Dover, L. G. (2000) Iron metabolism in pathogenic bacteria. Annu. Rev. Microbiol. **54**, 881–941
5 Braun, V. and Braun, M. (2002) Active transport of iron and siderophore antibiotics. Curr. Opin. Microbiol. **5**, 194–201
6 Faraldo-Gomez, J. D. and Sansom, M. S. P. (2003) Acquisition of siderophores in Gram-negative bacteria. Nat. Rev. Mol. Cell Biol. **4**, 105–116
7 Lower, S. K., Hochella, Jr, M. F. and Beveridge, T. J. (2001) Bacterial recognition of mineral surfaces: nanoscale interactions between *Shewanella* and α-FeOOH. Science (Washington, D.C.) **292**, 1360–1363
8 Mietzner, T. A., Tencza, S. B., Adhikari, P., Vaughan, K. G. and Nowalk, A. J. (1998) Fe(III) periplasm-to-cytosol transporters of Gram-negative pathogens. Curr. Top. Microbiol. Immunol. **225**, 113–135
9 Mietzner, T. A., Luginbuhl, G. H., Sandstrom, E. and Morse, S. A. (1984) Identification of an iron-regulated 37,000-Dalton protein in the cell envelope of *Neisseria gonorrhoeae*. Infect. Immun. **45**, 410–416
10 Khun, H. H., Kirby, S. D. and Lee, B. C. (1998) A *Neisseria meningitidis fbpABC* mutant is incapable of using nonheme iron for growth. Infect. Immun. **66**, 2330–2336
11 Bruns, C. M., Nowalk, A. J., Arvai, A. S., McTigue, M. A., Vaughan, K. G., Mietzner, T. A. and McRee, D. E. (1997) Structure of *Haemophilus influenzae* Fe^{3+}-binding protein reveals convergent evolution within a superfamily. Nat. Struct. Biol. **4**, 919–924
12 Taboy, C. H., Vaughan, K. G., Mietzner, T. A., Aisen, P. and Crumbliss, A. L. (2001) Fe^{3+} coordination and redox properties of a bacterial transferrin. J. Biol. Chem. **276**, 2719–2724
13 Guo, M., Harvey, I., Yang, W., Coghill, L., Campopiano, D. J., Parkinson, J. A., MacGillivray, R. T. A., Harris, W. R. and Sadler, P. J. (2003) Synergistic anion and metal binding to the ferric ion-binding protein from *Neisseria gonorrhoeae*. J. Biol. Chem. **278**, 2490–2502
14 Dhungana, S., Taboy, C. H., Anderson, D. S., Vaughan, K. G., Aisen, P., Mietzner, T. A. and Crumbliss, A. L. (2003) The influence of the synergistic anion on iron chelation by ferric binding protein, a bacterial transferrin. Proc. Natl. Acad. Sci. U.S.A. **100**, 3659–3664
15 Baker, H. M., Anderson, B. F. and Baker, E. N. (2003) Dealing with iron: common structural principles in proteins that transport iron and heme. Proc. Natl. Acad. Sci. U.S.A. **100**, 3579–3583
16 Alexeev, D., Zhu, H., Guo, M., Zhong, W., Hunter, D. J. B., Yang, W., Campopiano, D. J. and Sadler, P. J. (2003) A novel protein–mineral interface. Nat. Struct. Biol. **10**, 297–302
17 Ferreirós, C., Criado, M. T. and Gómez, J. A. (1999) The neisserial 37 kDa ferric binding protein (FbpA). Comp. Biochem. Physiol. B **123**, 1–7
18 Clegg, W., Powell, A. K. and Ware, M. J. (1984) Structure of trisodium bis(nitrilotriacetato)ferrate(III) pentahydrate, $Na_3[Fe\{N(CH_2CO_2)_3\}_2] \cdot 5H_2O$. Acta Crystallogr., Sect. C: Cryst. Struct. Commun. **40**, 1822–1824
19 Shweky, I., Bino, A., Goldberg, D. P. and Lippard, S. J. (1994) Syntheses, structures, and magnetic properties of two dinuclear iron(III) citrate complexes. Inorg. Chem. **33**, 5161–5162
20 Kabsch, W. (1993) Automatic processing of rotation diffraction data from crystals of initially unknown symmetry and cell constants. J. Appl. Crystallogr. **26**, 795–800
21 Otwinowski, Z. and Minor, W. (1997) Processing of X-ray diffraction data collected in oscillation mode. Methods Enzymol. **276**, 307–326
22 Alexeev, D. (2003) Twinning in presence of multiple NCS: metals in a bacterial transferrin. Acta Crystallogr., Sect. D: Biol. Crystallogr., in press
23 Deck, K. M., Tseng, T. A. and Burstyn, J. N. (2002) Triisopropyltriazacyclononane copper(II): an efficient phosphodiester hydrolysis catalyst and DNA cleavage agent. Inorg. Chem. **41**, 669–677
24 Ferguson, A. D., Chakraborty, R., Smith, B. S., Esser, L., van der Helm, D. and Deisenhofer, J. (2002) Structural basis of gating by the outer membrane transporter FecA. Science (Washington, D.C.) **295**, 1715–1719
25 Bino, A., Shweky, I., Cohen, S., Bauminger, E. R. and Lippard, S. J. (1998) A novel nonairon(III) citrate complex: a 'ferric triple-decker'. Inorg. Chem. **37**, 5168–5172
26 Goodwin, J. C., Sessoli, R., Gatteschi, D., Wernsdorfer, W., Powell, A. K. and Heath, S. L. (2000) Towards nanostructured arrays of single molecule magnets: new Fe_{19} oxyhydroxide clusters displaying high ground state spins and hysteresis. J. Chem. Soc. Dalton Trans. 1835–1840
27 Spiro, T. G., Pape, L. and Saltman, P. (1967) Hydrolytic polymerization of ferric citrate. I. Chemistry of the polymer. J. Am. Chem. Soc. **89**, 5555–5559
28 Shouldice, S. R., Dougan, D. R., Skene, R. J., Tari, L. W., McRee, D. E., Yu, R. and Schryvers, A. B. (2003) High resolution structure of an alternate form of the ferric ion binding protein from *Haemophilus influenzae*. J. Biol. Chem. **278**, 11513–11519
29 Mizutani, K., Yamashita, H., Kurokawa, H., Mikami, B. and Hirose, M. (1999) Alternative structural state of transferrin. The crystallographic analysis of iron-loaded but domain-opened ovotransferrin N-lobe. J. Biol. Chem. **274**, 10190–10194
30 Kuser, P., Hall, D. R., Haw, M., Neu, M., Evans, R. W. and Lindley, P. F. (2002) The mechanism of iron uptake by transferrins: the X-ray structures of the 18 kDa NII domain fragment of duck ovotransferrin and its nitrilotriacetate complex. Acta Crystallogr. D: Biol. Crystallogr. **58**, 777–783
31 Bruns, C. M., Anderson, D. S., Vaughan, K. G., Williams, P. A., Nowalk, A. J., McRee, D. E. and Mietzner, T. A. (2001) Crystallographic and biochemical analyses of the metal-free *Haemophilus influenzae* Fe^{3+}-binding protein. Biochemistry **40**, 15631–15637
32 He, Q.-Y., Mason, A. B., Woodworth, R. C., Tam, B. M., MacGillivray, R. T. A., Grady, J. K. and Chasteen, N. D. (1997) Inequivalence of the two tyrosine ligands in the N-lobe of human serum transferrin. Biochemistry **36**, 14853–14860
33 Kirby, A. J. and Younas, M. (1970) Reactivity of phosphate esters. Diester hydrolysis. J. Chem. Soc. B 510–513
34 Chin, J. and Zou, X. (1988) Cobalt(III) complex promoted hydrolysis of phosphate diesters: change in rate-determining step with change in phosphate diester reactivity. J. Am. Chem. Soc. **10**, 223–225
35 Butler, A. (2003) Iron acquisition: straight up and on the rocks? Nat. Struct. Biol. **10**, 240–241
36 Kurtz, D. M. (1997) Structural similarity and functional diversity in di-iron-oxo proteins. J. Biol. Inorg. Chem. **2**, 159–167

37 Theil, E. C. (1987) Ferritin: structure, gene regulation, and cellular function in animals, plants, and microorganisms. Annu. Rev. Biochem. **56**, 289–315
38 Chasteen, N. D. and Harrison, P. M. (1999) Mineralization in ferritin: an efficient means of iron storage. J. Struct. Biol. **126**, 182–194
39 Rees, D. C. and Howard, J. B. (2003) The interface between the biological and inorganic worlds: iron–sulfur metalloclusters. Science (Washington, D.C.) **300**, 929
40 Schroder, I., Johnson, E. and de Vries, S. (2003) Microbial ferric iron reductases. FEMS Microbiol. Rev. **27**, 427–447
41 Glasauer, S., Langley, S. and Beveridge, T. J. (2002) Intracellular iron minerals in a dissimilatory iron-reducing bacterium. Science (Washington, D.C.) **295**, 117–119
42 Zhong, W., Alexeev, D., Guo, M., Hunter, D. J. B., Campopiano, D. J. and Sadler, P. J. (2003) 7th International Symposium on Applied Bioinorganic Chemistry, abstract p18, Guanajuato, Mexico, April 1–5
43 Altschul, S. F., Madden, T. L., Schaffer, A. A., Zhang, J., Zhang, Z., Miller, W. and Lipman, D. J. (1997) Gapped BLAST and PSI-BLAST: a new generation of protein database search programs. Nucleic Acids Res. **25**, 3389–3402

Received 22 August 2003; accepted 16 September 2003
Published as BJ Immediate Publication 16 September 2003, DOI 10.1042/BJ20031283